

# Laser-ablation and induced nanoparticle synthesis

DIMITRI BATANI,<sup>1</sup> TOMMASO VINCI,<sup>2</sup> AND DAVIDE BLEINER<sup>3</sup>

<sup>1</sup>Université Bordeaux, CNRS, CEA, CELIA (Centre Lasers Intenses et Applications), UMR 5107, Talence, France

<sup>2</sup>LULI, Ecole Polytechnique, Palaiseau, France

<sup>3</sup>Institute for Applied Physics, University of Bern, Berne, Switzerland

(RECEIVED 19 June 2013; ACCEPTED 22 July 2013)

## Abstract

Laser pulses are largely used for processing and analysis of materials and in particular for nano-particle synthesis. This paper addresses fundamentals of the generation of nano-materials following specific thermodynamic paths of the irradiated material. Computer simulations using the hydro code MULTI and the SESAME equation of state have been performed to follow the dynamics of a target initially heated by a short laser pulse over a distance comparable to the metal skin depth.

**Keywords:** Bimodal curve; Equation of state; Heterogeneous boiling; Laser assisted nano-particle synthesis; Phase explosion; Phase transitions; Spinodal curve

## 1. INTRODUCTION

Laser irradiation of matter is largely used for *processing* as well as for the *diagnostics* of materials, allowing relatively simple operation and versatility. Also, laser irradiation allows getting extreme conditions in irradiated matter. Extreme states of matter, lying at the edge between warm solid matter and ideal plasmas, are obtained in common applications, such as laser ablation, nano-machining, nano-structuring, etc. (see for instance, Bussoli *et al.*, 2007; Batani *et al.*, 2003; Di Bernardo *et al.*, 2003; Trtica *et al.*, 2006; Batani, 2010; Gamaly *et al.*, 2002).

Due to the high laser intensity, these processes usually involve the formation of plasma on the surface of the irradiated targets, which results in laser ablation, i.e., in the removal of material from the surface. Such material forms an ablation plume and can then be deposited on particular substrates placed at some distance from the irradiation point. This technique is known as *pulsed laser deposition* (Chrisey *et al.*, 1994; Willmott, 2004; Greer *et al.*, 1997) in which a stoichiometric vapor from irradiated targets of known composition is deposited as a stoichiometric thin film upon a substrate, in order to engineer layers with tailored optical, electrical or mechanical properties.

Under particular conditions, the ablation of matter and plume expansion involve the synthesis of nano-particles

Such laser-assisted synthesis, “simply” obtained by irradiating a target and generating an aerosol, is a growing and attractive technique (Kokai *et al.*, 2005; Scott *et al.*, 2001; Huisken *et al.*, 2000; Cai *et al.*, 1998; Becker *et al.*, 1998; Márton *et al.*, 2003; Fazio *et al.*, 2009).

*Traditional techniques* for nano-particle synthesis have made lot of progress but still show weaknesses. Mainly, two methods have dominated the field, namely *gas phase synthesis* and *sol-gel processing*. Gas-phase methods include synthesis by combustion flame (Zachariah, 1994; Calcote & Keil, 1997; Axelbaum, 1997; Pratsinis, 1997); plasma (Rao *et al.*, 1997); chemical vapor condensation (Kear *et al.*, 1997); spray pyrolysis (Messing *et al.*, 1994); electrospray (De la Mora *et al.*, 1994); and plasma spray (Berndt *et al.*, 1997). Sol-gel processing is a wet chemical synthesis approach that can be used to generate nano-particles by gelation, precipitation, and hydrothermal treatment (Kung & Ko, 1996). Both methods have indeed been able to generate nano-particles with diameters down to a few nm (reported size variances are  $\sim 20\%$ ) with consistent crystal structure, surface deprivatization, and a high degree of mono-dispersion. However, the most challenging problems remains the generation of *monodispersed batches*, i.e., to get control on the primary size variances such that size filtration (e.g., centrifugal or mobility classification) is not necessary. Gas-phase synthesis methods have shown the best size mono-dispersity. Besides size dispersion, another major challenge is that of high volume yields. Indeed gas-phase synthesis is generally a low yield process (typically in the range of

Address correspondence and reprint requests to: Dimitri Batani, University Bordeaux, CEA, CNRS, Centre Laser Intense et Applications, UMR 5107, F-33405 Talence, France. E-mail: [batani@celia.u-bordeaux1.fr](mailto:batani@celia.u-bordeaux1.fr)

0.1 g/hr). For sol-gel processing, issues concerning the cost and purity of precursors and the handling of hazardous solvent are to be considered in addition.

Laser-assisted synthesis of nano-particle from a laser-induced plume is an example *one-step process*. One of its main advantages is that of batch *purity*. Some production methods, such as mechanical milling and grinding, or chemical generation methods like the sol-gel process present contamination risks. For gas-phase methods, the purity of the aerosol product depends primarily on that of the carrier gas and the vessel material. In laser-assisted synthesis, the laser beam is focused directly on the target, and then external contamination is practically non-existent.

A second point is that of *preparation time*, and the number of required steps. Laser ablation is a one-step procedure that can lead directly, under optimized setup, to ready-to-use batches, without any additional sorting procedures required. Laser ablation allows also flexible control over the ablated mass by varying the pulse energy and repetition rate. Multi-component and stoichiometric aerosols can be easily generated by appropriate selection of the target material. In fact, pulsed laser ablation offers access to an unlimited nano-material spectrum, since the nano-particles may be generated from direct ablation of almost any solid material. The produced nano-particles, if ablated in a liquid, can be easily turned into a colloidal system or functionalized by specific surface reactions. Last but not least, the handling of solid targets for the laser-ablation is easier and less hazardous than using metal organic compounds or compounds containing halogenides. Avoiding the use of toxic, hazardous, or pyrophoric chemical precursors for nanomaterial synthesis is also an environmental-friendly (“green”) practice.

The present paper will review the advantages of using laser ablation for the generation of nano-particles following a specific thermodynamic path of the irradiated material and we will discuss the physics of the process in detail.

## 2. LASER-MATTER INTERACTION AND LASER ABLATION

A high intensity laser ( $I \gg 1 \text{ GW/cm}^2$ ) irradiating a solid target, triggers a number of effects, which are summarized as follows:

1. *Optical effects*, which are all processes that involve radiative phenomena such as absorption, reflection, etc. At very high intensity ( $I > 1 \text{ TW/cm}^2$ ) these effects behave non-linearly;
2. *Thermal effects*, which are all processes, activated by a change in temperature such melting, vaporization, etc. At very high heating rates the material may not “follow” the temperature curve and thus be metastable;
3. *Further physical effects*. Depending on the boundary conditions, the laser ablation process can be described considering a number of additional ad hoc effects. For instance, mechanical effects, which are strain/stress

processes activated within the irradiated body. Physical-chemical effects are all processes involving compositional modification either overcoming activation barriers or inducing fractional transport.

All these multiple processes may co-exist and overlap depending on operating conditions (Bleiner & Bogaerts, 2006) Depending on the boundary conditions, length-scales and time-scale may vary and involve different outcomes. It is thus essential to have a vision for the length- and time-scales involved.

The laser energy interacts with the *bound* (dielectrics) or *free* (conductors) electrons and initiates a perturbation over an initial thickness  $\delta$  of the order of the laser skin depth. The next step is the description of the penetration of the absorbed energy in the material at a distance  $l$ , from the initially heated region.

Depending on the *electron-phonon coupling* time-scale and the laser pulse time scale, the processes can have different evolutions. In the case of rapid (within the pulse time-scale) equilibration, the electrons and atoms temperature become indistinguishable and one can describe the laser-matter interaction with a *collective (hydrodynamic) description*. This permits the use of thermo-optical properties and macroscopic equations that define the state of the target in radiative continuity with the laser source. In this case, local thermal equilibrium (LTE) is a viable assumption that can be adopted. If, however, the electron excitation is much faster than the thermalization time, a two-temperature model (TTM) is necessary (Zhigilei & Garris, 1999) (Perez & Lewis, 2003).

The TTM describes a non-equilibrium state between electrons and the lattice. When an ultrafast EM field is applied to a metallic sample, a state of thermal mismatch between electrons and the lattice is induced for a short transient time. This problem was solved in the 1950s (Ginzburg & Shabanskii, 1955) in the high temperature limit, i.e., for temperatures much higher than the so-called *Debye temperature* ( $T_D = \hbar v/k$ ) of the irradiated material. The complete solution for arbitrary temperatures was given in (Kaganov et al., 1957). Later, the model was revised (Nolte et al., 1996; Kanavin et al., 1998), and despite several refinements it still remains the “standard model” of short-pulse laser ablation.

TTM assumes “instantaneous” thermalization of non-thermal electron distribution to a hot Fermi distribution, and then this hot Fermi distribution cools through electron-phonon interactions with the phonon subsystem. The assumption of “*instantaneous thermalization*” or “*adiabatic assumption*” is, in general, not in agreement with some experimental observations. Thus, the TTM is clearly inadequate to account for non-thermal electron distributions. To consider the non-equilibrium electron kinetics (non-thermal part), a stochastic kinetic model may be used.

For *ns*-pulse irradiation, LTE can be assumed, and the time-dependent temperature distribution in the target depth can be described by the heat-conduction equation (*Fourier*

law), that in one-dimensional form is written as follows:

$$c_p \rho \left( \frac{\partial T(z, t)}{\partial t} - u(t) \frac{\partial T(z, t)}{\partial z} \right) = \frac{\partial}{\partial z} \lambda \frac{\partial T(z, t)}{\partial z} + |1 - \chi| \alpha I(t) e^{-\alpha z}, \quad (1)$$

where  $T$  is the temperature in the material at depth  $z$  and time  $t$ ,  $I$  is the laser intensity,  $u(t)$  is the velocity of surface recession per unit pulse and  $c_p$  is the heat capacity at constant pressure,  $\lambda$  is the thermal conductivity,  $\rho$  is the target density,  $\chi$  is the target reflectivity,  $\alpha$  is the absorption coefficient. For non-isotropic condition, two-dimensional or even three-dimensional versions of Eq. (3) are needed.

The calculated value of  $u(t)$  depends on the specific mechanisms taken into account, as described below.

*Surface Vaporization* involves an activated migration of surface particles away from the condensed phase into the ambient. The rate of vapor pressure change as a function of temperature along phase boundaries is given by the well-known Clausius-Clapeyron equation, which determines the so-called *binodal line* (Fig. 1). For a constant enthalpy across the temperature range from  $T_b$  and  $T_s$ , the integrated form is as follows:

$$p(T_s) = p_o \exp \left[ \frac{\Delta H}{R} \left( \frac{1}{T_o} - \frac{1}{T_s} \right) \right], \quad (2)$$

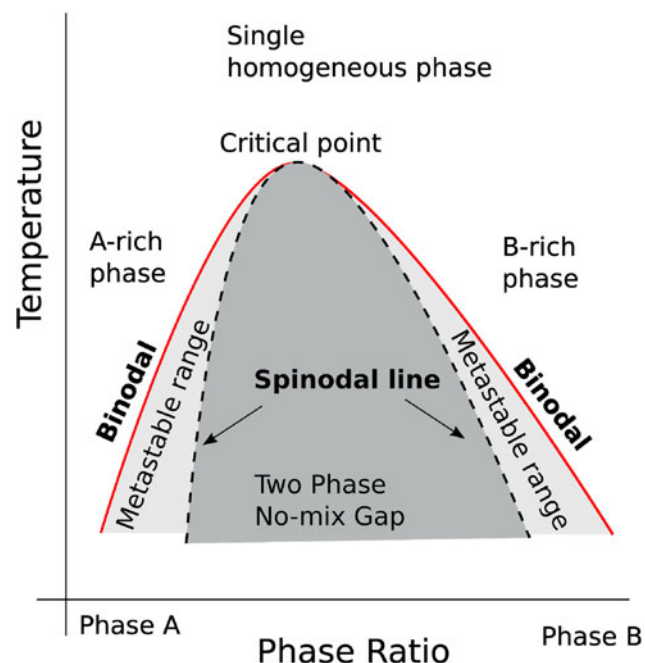


**Fig. 1.** (Color online) Qualitative phase stability diagram with temperature vs. phase mixture composition. From a homogeneous phase the system can split-up into distinguished phase at lower temperatures. If the phases are close to the binodal line these can be partially co-existing in a mix. Moving beyond the spinodal line, into the miscibility gap, the phases will immediately separate.

here  $p$  is the pressure at temperature  $T_s$ ,  $p_o$  is the ambient pressure,  $\Delta H$  is the enthalpy of phase transition,  $R$  is the ideal gas constant,  $T_o$  and  $T_s$  are, respectively, the temperatures at the initial state (standard conditions) and at saturation (i.e., at the binodal boundary).

The binodal line is represented in Figure 1, which shows to separate the different phases of the system (e.g., a Van der Waals gas as well as a metal). The spinodal curve (Liley, 2000) delimits the miscibility range, i.e., the metastable range where two phases can co-exist, one being super-heated.

The velocity of surface recession was derived (Miotello & Kelly, 1995) from the Hertz-Knudsen equation, inserting Eq. (2) in the pressure term, and multiplying by the vaporization coefficient  $\xi$  and the volume  $m/\rho$ . After rearranging, the recession velocity is expressed as follows:

$$u(T_s) = \frac{\partial z}{\partial t} = \xi \frac{p_o}{\rho} \sqrt{\frac{m}{2\pi k T_s}} \exp \left[ \frac{\Delta H}{R} \left( \frac{1}{T_o} - \frac{1}{T_s} \right) \right], \quad (3)$$

where one notes that the dependency on  $T_s$  is not monotone, due to the combined effect of the pre-exponential (*back-flux*) and the exponential term (*forward-flux*). At high surface temperatures the process is increasingly less efficient and at very high temperature the surface recession velocity slightly decreases with laser irradiance, as shown before (Wang *et al.*, 2007).

*Heterogeneous boiling* involves an activated migration of particles from the condensed phase into a volatile phase, similarly to surface vaporization, yet the process here occurs *within* the body of the condensed phase with formation of bubbles. The presence of *heterogeneous nuclei* disseminated in the irradiated volume should favor the formation of individual bubbles. Indeed, such impurities lower the activation energy. The bubbles may grow beyond a critical size (Bleiner, 2005) and coalesce by diffusion, thus causing extensive boiling (Kandlikar). The heterogeneous nucleation rate  $J_{het}$  per unit volume is obtained from the Volmer-Döring formula, as given in Blander and Katz (1975)

$$J_{het} = n_{het} Q \sqrt{\frac{2\gamma}{\pi m F}} \exp \left[ -\frac{16\pi\gamma^3 F}{3kT(p_b - p_o)^2} \right] \quad (4)$$

where  $Q$  and  $F$  are two specific control parameters that depend on the geometry of the heterogeneous nuclei and where  $n_{het}$  is the heterogeneous nuclei number density,  $m$  is the atomic/molecular mass,  $p_b$  is the bubble pressure,  $p_o$  is the ambient pressure as before. The surface tension  $\gamma$  is a function of temperature, which complicates the application of the equation. Heterogeneous boiling is retained to be not so relevant for ultrashort laser pulse durations because of *time-dependent* probability of nuclei formation and bubble diffusion and coalescence (Kleinert, 1997).

*Homogeneous boiling* is finally the explosive boiling of a super-heated target material, due to a rapid state transition,

i.e., *metastable/unstable/stable*, occurring close to the critical temperature. This process leads to the release of a mixture of vapor and droplets that has been also termed “gas of droplets” or “phase explosion” (Martynyuk, 1978; 1983; Xu, 2002). Figure 2 shows the  $T$ - $p$  phase stability diagram for any arbitrary molten metallic substance.

The axes are plotted in terms of reduced temperature and pressure, i.e., relative to the critical point values. The binodal line is the thermodynamic equilibrium boundary that separates co-existing liquid and vapor phase for a given combination of  $p$  and  $T$ . The binodal line can be rapidly crossed for very fast laser pulses, because the induced heating is kinetically too rapid. In this situation, a superheated melt is obtained (grey region in Fig. 2), which retains the features of a liquid as long as it is metastable. The limit for metastability is the spinodal line, where the liquid collapses. The homogeneous nucleation rate per unit volume  $J_{hom}$  is given by the following equation (Blander & Katz, 1975):

$$J_{hom} = n_{hom} \sqrt{\frac{2\gamma}{\pi m}} \exp\left[-\frac{16\pi\gamma^3}{3kT(p_b - p_o)^2}\right], \quad (5)$$

where  $n_{hom}$  is the number density of homogeneous nuclei (Miotello & Kelly, 1995; Xu, 2002). [53] B (Rethfeld et al., 2002) discussed about the *time scale* for realization of explosive boiling (spinodal breakdown), i.e., the temporal interval it takes to have the irradiated zone filled with homogeneous nucleation bubbles. The process is probably realistic for fs laser pulses, but there have been a few claims on

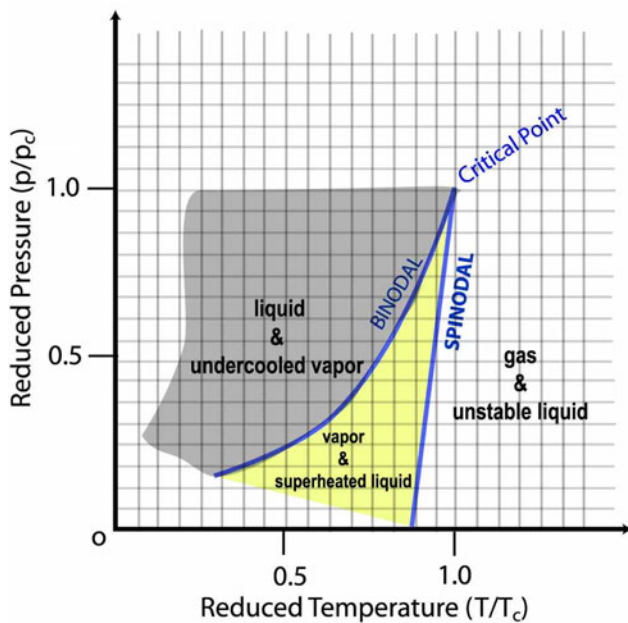


Fig. 2. (Color online) Qualitative phase stability diagram of a liquid metal near the critical point, with pressure vs. temperature dependency. For fast heating, as obtained during laser ablation, the melt can be pushed close to critical conditions (superheating), which favors the realization of explosive boiling.

experimental evidences of spinodal breakdown *even* at ns pulse durations (Geoghan, 1993; Song, 1998). Also Bulgakova and Bulgakov (2001) as well as Russo et al. (2004) showed plots with the ablation rate as a function of laser fluence, from where one could see that there is a threshold value for rapid increase of the dependency. This increase is attributed to the transition from a normal vaporization regime into a regime of phase explosion. At low pulse energies only clusters and atomic particles are emitted (Semaltianos et al., 2010), whereas for pulse energies above a certain (material-dependent) value, liquid droplets are also ejected.

Thus, particles size measurements have shown *in general* that ns-pulses lead to bimodal distributions, with one mode around 30–70 nm that is attributed to vapor condensation and a second mode around 0.5–10  $\mu\text{m}$ , attributed to splashing of molten droplets or mechanical shrapnel. The composition of the particles is also influenced by the presence of a reactive ambient, e.g., partial pressure of oxygen, liquid immersion, etc. The sticking of nanoparticle in chain-like assembly has been mitigated with the use of immersion in surfactants.

The main difference between ablation in air and in liquid is that the latter produces a stronger confinement of the expanding plume, which affects the thermodynamic and kinetic properties and the evolution of products. Besides, the formation of bubbles by means of cavitation in the liquid is also to be considered, which affect the reproducibility and size variance. Then, the plume confinement favors a stronger re-interaction of the particles with the trailing edge of the laser pulse. This leads to a further reduction of the final particle size and a narrowing of the size spread. This possibility of “tuning” the nanoparticle size distribution by adjusting the ablation time duration was demonstrated in (Semaltianos et al., 2010).

### 3. NUMERICAL SIMULATIONS

In order to test the previous scenario for nano-particle synthesis, we have done some computer simulations using the hydrodynamics code MULTI (Ramis et al., 1998). MULTI is a classical code used for simulating laser-matter interaction in the ns-regime although an fs-version has also been developed (Eidmann et al., 2000). Nevertheless in the present simulations we didn’t use MULTI to simulate the laser-plasma interaction step, but just to simulate the expansion phase.

Therefore, we considered a thick Al target (50  $\mu\text{m}$ ) and uniformly heated a thickness of 100 nm of solid density Al to an initial temperature  $T$ , of the order of a few eV. This is consistent with the previous picture of the first phase of laser-ablation with short-pulse laser as being a rapid heating of the target material at practically constant density (hydrodynamics has no time to act on the short time scale of the laser pulse) over a distance comparable to the laser penetration skin depth. Al was used in these simulations just because, in comparison with other materials, its equation of state in

the megabar regime is rather better known. One must consider indeed that heating solid density Al to  $T \approx 1$  eV ( $\approx 11000$  K) produces a pressure of the order of 10 GPa. This shows indeed that, as we said before, laser irradiation of materials is a simple way of creating *extreme states of matter* (warm dense matter).

The equation of state of Al used in the code is the SESAME table (Barnes & Lyon, 1989) developed at the Los Alamos National Laboratory in the United States. The phase diagram of the SESAME table used in our simulations is shown in Figure 3.

Although it may not accurately describe all the states of Al in this regime (a complete thermo dynamical description of warm dense matter states is still far to be obtained), this does not jeopardize the results of our numerical simulations since we are only interested in internal consistency of our scenario here.

The results of some of the numerical simulations we performed are represented in Figures 4, 5, and 6. Notice that in such simulations the material was uniformly heated to  $T = 5$  eV but the curves, which are shown, are neither uniform nor show such value of temperature. This is due to three different effects: (1) the fact that in the simulations we only heat the electrons (again consistently with our scenario of short-pulse laser ablation), (2) the rapid cooling following expansion, and (3) the thermal conduction towards the cold solid material behind the heated target which, although practically non active during the laser pulse, is indeed pretty effective on the time scale of plasma expansion shown in the simulations.

In the first picture (Fig. 4), each line represent the whole heated part of the target (on the right the expanded part, on the left one the compressed part), and each single point of the line represents a single cell of the mesh used in the simulations (400 cells were used for simulating the target: 200 for

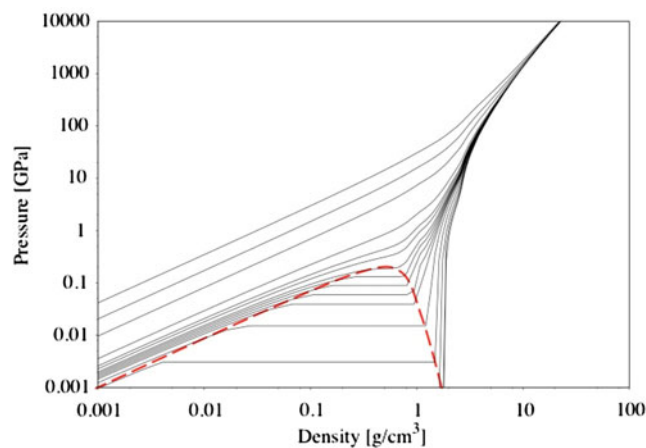


**Fig. 3.** (Color online) Phase diagram of Al following the SESAME table 3719. The curves A to Z represents the isotherms and respectively corresponds to temperature values from 0 to 46400 K. For sake of clarity the bimodal curve separating the various phases has been added (red dashed curve). The critical isotherm here corresponds to a temperature of 5800 K.

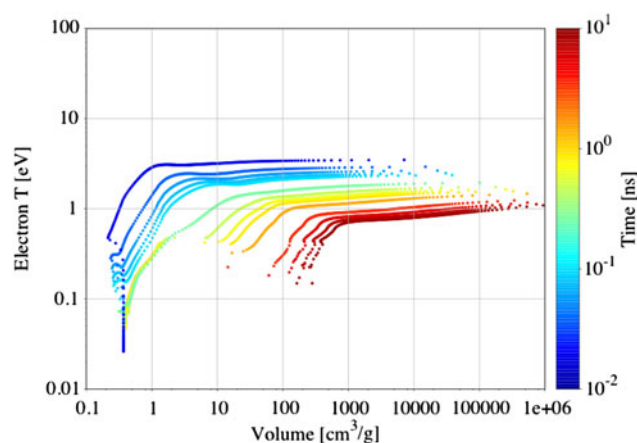


**Fig. 4.** (Color online) Cooling and expansion of the material following an instantaneous isochoric and uniform heating of the first layer. Each line in the  $(V, T)$  plane represents the whole heated part of the target (on the right the expanded part, on the left one the compressed part), and each single point of the line represents a single cell of the mesh used in the simulations.

the cold and 200 for the “hot” part with a geometrical progression thickness of 1.0331 and 1.025, respectively, resulting in the first cell thickness of 0.018 nm). As time changes (represented by the change of color) each cell changes its temperature and its specific volume ( $1/\rho$  measured in  $\text{cm}^3/\text{g}$ , where  $\rho$  is the material density). The cold cells of the deep material are all represented by a single point at  $\rho = 2.7 \text{ g/cm}^3$  and  $T = 0.025$  eV (the initial temperature used in the simulations) and therefore is outside the graph. We see that the material is getting colder everywhere but the vapour phase (low density, large volumes) gets cooler in an approximate uniform way, while larger temperature gradients are present in the dense part. Also, we see the typical “bell shape” connected to the presence of the phase of coexistence between the various phases.

The following two figures (5 and 6) represent the same simulations but superimposed to the phase diagram from the sesame tables (previous Fig. 3). In the first one, again,

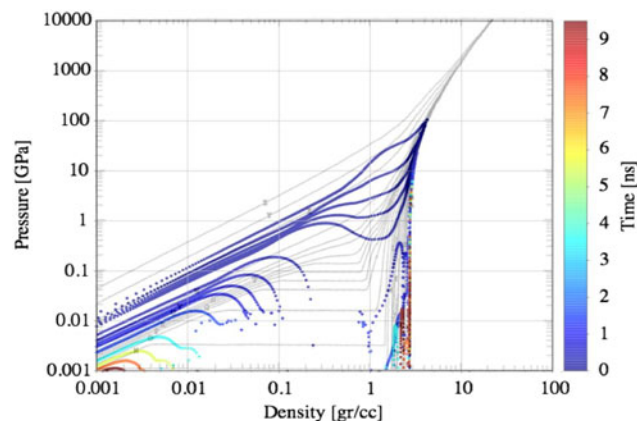


**Fig. 5.** (Color online) The same as Figure 8 but in the  $(\rho, P)$  plane superimposed to the phase diagram from the Sesame tables (Fig. 3).

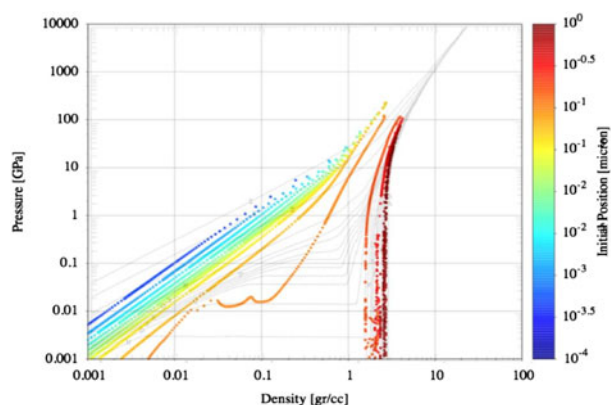


**Fig. 6.** (Color online) Cooling and expansion of the material following an instantaneous isochoric and uniform heating of the first layer. Each line represent the time evolution of a single cell in the simulation mesh, i.e., the time evolution of a part of the target in the  $(\rho, P)$  plane. Super-imposed the phase diagram from the Sesame tables (Fig. 3)

each line represents the state of all the heated region of the target at different times. As the material cools down, significant regions of the targets enter the bistable region.

Figure 6 instead shows the time evolution of each point each cell of the target mesh and it shows therefore the cooling of material. Here the initial temperature is sufficient to bring the material isochorically to a plasma state (i.e., from the initial state, along vertical line, to a temperature above the critical isotherm which separates the liquid/liquid phases from the gas phases). Later they cool down while remaining in He gas phases. In this case, the condensation of the material may occur at later times when the external regions of the targets reach low temperatures (below the critical isotherm again) following their adiabatic cooling (as obvious, Fig. 10 clearly shows that such adiabats are steeper than isotherms).

The internal regions of the targets instead cool because of thermal conduction to the deeper cold material and when they finally expand they go along a different trajectory, which keep them in the liquid phase, or, rather, bring them through the metastable region allowing for the phenomenon of phase explosion (notice in particular the orange line in Fig. 10).

[Let's notice that in a real case, the internal target region will be already cooler than those more external, due to the exponential penetration of laser light in the materials following Beer's law].

#### 4. CONCLUSIONS

In this paper we have described the principles of laser-ablation and of nanoparticle production by laser-ablation. The description of laser ablation has been mainly concentrated on the use of short pulses through an analysis of the Two-Temperature Model. We have also outlined the changes, which are needed when high laser intensities are used. Concerning nanoparticle production we have described

the mechanism of phase explosion which is in particular possible when the heated material follows particular thermodynamic paths during its cooling. The description we have made holds in vacuum, while today laser-ablation in liquid seems to be a preferential path to nanoparticle production. However the thermodynamic principles, which we have outlined, hold in general, the presence of the liquid probably simply affecting the conditions for cooling of the expanding materials.

#### ACKNOWLEDGEMENT

D. Bleiner's team has been supported by the Swiss National Science Foundation under the grant number PP00P2-133564/1.

#### REFERENCES

- AXELBAUM, R.L. (1997). "Developments in sodium/halide flame technology for the synthesis of unagglomerated non-oxide nanoparticles." In *Proc. of the Joint NSF-NIST Conference on Nanoparticles: Synthesis, Processing into Functional Nanostructures and Characterization*. May 12–13, Arlington, VA.
- BARNES, J. & LYON, S. (1989). SESAME EOS table 3719 for Aluminum
- BATANI, D., H. STABILE, A. RAVASIO, G. LUCCHINI, J. ULLSCHMIED, E. KROUSKY, L. JUHA, J. SKALA, B. KRALIKOVA, M. PFEIFER, C. KADLEC, T. MOCEK, A. PRÁG, H. NISHIMURA, Y. OCHI. (2003). "Ablation Pressure Scaling at Short Laser Wavelength" *Physical Review E*, **68**, 067403.
- BATANI, D. (2010). "Short-pulse laser ablation of materials at high intensities: influence of plasma effects" *Laser and Particle Beams*, **28**, 235.
- BECKER, M. F., J. R. BROCK, HONG CAI, D. E. HENNEKE, J. W. KETO, JAEMYOUNG LEE, W. T. NICHOLS & H. D. GLICKSMAN. (1998). "Metal nano-particles generated by laser ablation" *Nanostruct. Mater.* **10**, 853–863.
- BERNDT, C.C., J. KARTHIKEYAN, T. CHRASKA, & A.H. KING. (1997). "Plasma spray synthesis of nanozirconia powder" in *Proc. of the Joint NSF-NIST Conf. on Nanoparticles*.
- BLANDER, M., J.L. KATZ. (1975). "Bubble nucleation in liquids" *Amer. Inst. Chem. Eng. (AIChE) Journal*, **21**, 833–848.
- BLEINER, D. & ANNEMIE BOGAERTS. (2006). "Multiplicity and contiguity of ablation mechanisms in laser-assisted analytical micro-sampling" *Spectrochimica Acta Part B* **61**, 421–432.
- BLEINER, D. (2005). "Mathematical modelling of laser-induced particulate formation in direct solid microanalysis, *Spectroch. Acta B* **60**, 49–64.
- BULGAKOVA, NM, AV BULGAKOV. (2001). "Pulsed laser ablation of solids: transition from normal vaporization to phase explosion" *Appl. Phys. A* **73**, 199.
- BUSSOLI MARCO, DIMITRI BATANI, MARZIALE MILANI, MILAN TRTICA, BILJANA GAKOVIC, EDOUARD KROUSKY. (2007). "Study of Laser Induced Ablation with FIB Devices" *Laser and Particle Beams*, Volume **25**, Issue 01, pp 121–125
- CAI, H., N. CHAUDHARY, J. LEE, M. F. BECKER, J. R. BROCK & J. W. KETO. (1998). "Generation of metal nanoparticles by laser ablation of microspheres" *J. Aerosol Sci.* **29**, 627–636.

- CALCOTE, H.F., & D.G. KEIL. (1997). "Combustion synthesis of silicon carbide powder" in *Proc. of the Joint NSF-NIST Conf. on Nanoparticles*.
- Chrissey, D.B., G.K. Hubler. (eds.) (1994). "Pulsed laser deposition of thin films" Wiley-Interscience, New-York
- DE LA MORA, J.F., I.G. LOSCERTALES, J. ROSELL-LLOMPART, K. SERAGELDIN, & S. BROWN. (1994). "Electrospray atomizers and ultrafine particles" in *Proc. Joint NSF-NIST Conf. on UltraFine Particle Engineering* (May 25–27, 1994, Arlington, VA)
- DI BERNARDO, A., D. BATANI, C. COURTOIS, B. CROS, G. MATTHIEUSSENT. (2003). "High Intensity Ultra short laser induced ablation of metal targets in the presence of ambient gas" *Laser and Particle Beams*, **21**, 59–64 (2003).
- EIDMANN, K., MEYER-TER-VEHN, J., SCHLEGEL, T., HÜLLER, S. (2000). *PRE*, **62**, 1202.
- FAZIO, E., F. NERI, P.M. OSSI, N. SANTO & S. TRUSSO. (2009). "Ag nanocluster synthesis by laser ablation in Ar atmosphere: A plume dynamics analysis" *Laser and Particle Beams*, Volume **27**, Issue 02, pp 281–290
- GAMALY, E.G. A.V. RODE, B. LUTHER-DAVIES, V.T. TIKHONCHUK. (2002). "Ablation of solids by femtosecond lasers: Ablation mechanism and ablation thresholds for metals and dielectrics" *Physics of Plasmas* **9** (3), 949–957.
- GEOGHAN, DB (1993). "Imaging and blackbody emission spectra of particulates generated in the KrF-laser ablation of BN and  $\text{YBa}_2\text{Cu}_3\text{O}_{7-x}$ " *Appl Phys Lett* **62**, 1463–1465.
- GINZBURG, V.L. & V.P. SHABANSKII. (1955). *Dokl. Akad. Nauk SSSR* **100**, 445.
- GREER, L.A., M.D. TABAT, C. LU. (1997). "Future trends for large-area pulsed laser deposition" *Nuclear Instr. Meth. Phys. Res. B* **121**, 357
- HUISKEN, F., H. HOFMEISTER, B. KOHN, M.A. LAGUNA & V. PAILLARD. (2000). "Laser production and deposition of light-emitting silicon nanoparticles" *Appl. Surf. Sci.*, 154–155, 305–313.
- KAGANOV, M.I., I.M. LIFSHITZ, & L.V. TANATAROV. (1957). *Zh. Eksp. Teor. fiz.* **31**, 232 [Sov. Phys. JETP 4, 173 (1957)].
- KANAVIN, A.P. et al.. (1998). *Phys. Rev. B*, **57**(23), 14698
- Kandlikar, S.G., M. Shoji, V.K. Dhir. (Editors) (1999). "Handbook of phase changes" Taylor & Francis Group
- KEAR, B.H., R.K. SADANGI, & S.C. LIAO. (1997). "Synthesis of WC/Co/diamond nanocomposites" in *Proc. of the Joint NSF-NIST Conf. on Nanoparticles*.
- KLEINERT, H. (1997). "Gauge fields in condensed matter" Vol. **II**, pp. 743–1456.
- KOKAI, F., A. KOSHIO, M. SHIRAIISHI, T. MATSUTA, S. SHIMODA, M. ISHIHARA, Y. KOGA, H. DENO. (2005). "Modification of carbon nanotubes by laser ablation" *Diamond And Related Materials* **14**, 724–728.
- KUNG, H.H., & E.I. KO. (1996). *Chem. Eng. J.* **64**, 203.
- LILEY, P.E. (2000). "The spinodal for a Van der Waals fluid", *International Journal of Mechanical Engineering Education* Vol **30** No 2.
- MARTYNYUK, MM. (1978). "Phase explosion of a metastable fluid" *Comb. Expl. & Shock Waves* **13**, 178–191.
- MARTYNYUK, MM. (1983). "Critical point parameters of metals" *Russ. J. Phys. Chem.* **57**, 810–821.
- MÁRTON, Zs. L. LANDSTRÖM, M. BOMAN & P. HESZLER. (2003). "A comparative study of size distribution of nanoparticles generated by laser ablation of graphite and tungsten" *Mater. Sci. and Eng. C* **23**, 225–228.
- MESSING, G.L., S. ZHANG, U. SELVARAJ, R.J. SANTORO, & T. NI. (1994). "Synthesis of composite particles by spray pyrolysis" in *Proc. of the Joint NSF-NIST Conf. on Ultrafine Particle Engineering* (May 25–27, Arlington, VA).
- MIOTELLO, A., R KELLY. (1995). "Critical assessment of thermal models for laser sputtering at high fluences" *App. Phys. Lett.* **67** 3535–3537
- NOLTE, S., et al. (1996). *J Opt. soc. Am.B*, **14**(10), 2716
- PEREZ DANNY & LAURENT J. LEWIS. (2003) "Molecular-dynamics study of ablation of solids under femtosecond laser pulses" *Phys. Rev. B* **67**, 184102.
- PRATSINIS, S.E. (1997). "Precision synthesis of nanostructured particles" in *Proc. of the Joint NSF-NIST Conf. on Nanoparticles*.
- RAMIS, R., SCHMALZ, R. & MEYER-TER-VEHN, J. (1988). "MULTI A computer code for one-dimensional multigroup radiation hydro-dynamics" *Computer Physics Communications* **49**, p. 475–505.
- RAO, N.P., N. TYMIK, J. BLUM, A. NEUMAN, H.J. LEE, S.L. GIRSHICK, P.H. McMURRY, & J. HEBERLEIN. (1997). "Nanostructured materials production by hypersonic plasma particle deposition" in *Proc. of the Joint NSF-NIST Conf. on Nanoparticles*.
- RETHFELD, B., K SOKOLOWSKI-TINTEN, D VON DER LINDE, SI ANISIMOV. (2002). "Ultrafast thermal melting of laser-excited solids by homogeneous nucleation" *Phys. Rev. B*, **65**, 092103.
- RUSSO, R.E., X.L. MAO, C. LIU & J. GONZALEZ. (2004). "Laser assisted plasma spectrochemistry: laser ablation" *J. Anal. Atom. Spectrom.* **19**, 1084–1089.
- SCOTT, C.D., S. AREPALLI, P. NIKOLAEV, R.E. SMALLEY. (2001). "Growth mechanisms for single-wall carbon nanotubes in a laser-ablation process" *Appl. Phys. A: Mater. Sci. & Proc.* **72**, 573–580.
- SEMALTIANOS, LOGOTHETIDIS, PERRIE, ROMANI, POTTER, EDWARDSON, FRENCH, SHARP, DEARDEN, WATKINS, J. (2010). *Nanopart. Res.* **12**, 573.
- SONG, KH, X XU. (1998). "Explosive phase transformation in excimer laser ablation" *Appl. Surf. Sci.* **127–129**, 111.
- TRTICA, M., GAKOVIC, B., MARAVIC, D., BATANI, D., & REDAELLI R. (2006). "Surface Modification of Titanium by High Intensity Ultra-short Nd:YAG Laser", *Mater. Sci. Forum*, **518**, 167–172.
- XU, X. (2002). Phase explosion and its time lag in nanosecond laser ablation. *Appl. Surf. Sci.* **197–198**, 61–66.
- WANG YING-LONG, WEI XU, YANG ZHOU, LI-ZHI CHU and GUANG-SHENG, FU. (2007). "Influence of pulse repetition rate on the average size of silicon nanoparticles deposited by laser ablation" *Laser and Particle Beams*, Volume **25**, Issue 01, Mar, pp 9–13
- WILLMOTT, P.R. (2004). "Deposition of complex multielemental thin films." *Prog. Surf. Sci.* **76**, 163.
- ZACHARIAH, M.R. (1994). Flame processing, in-situ characterization, and atomistic modeling of nanoparticles in the reacting flow group at NIST. In *Proc. of the Joint NSF-NIST Conf. on Ultra-fine Particle Engineering*. May 25–27, Arlington, VA.
- ZHIGILEI, LEONID V. & GARRIS, BARBARA, J. (1999). Molecular dynamics simulation study of the fluence dependence of particle yield and plume composition in laser desorption and ablation of organic solids. *Appl. Phys. Lett.* **74**, 134.